Ion Energy Dependence of Dry Etch Damage Depth in Ga_2O_3 Schottky Rectifiers

Chao-Ching Chiang[1], Xinyi Xia[1], Jian-Sian Li[1], Fan Ren[1] and S.J. Pearton[2]

[1] Department of Chemical Engineering, University of Florida, Gainesville, FL 32606 USA

[2] Department of Materials Science and Engineering, University of Florida, Gainesville, FL 32606 USA

ABSTRACT

Dry etch damage in β-Ga_2O_3 is manifested by a reduction in near-surface carrier concentration, possibly due to the introduction of Ga_v acceptor states. The depth to which the carrier density is affected is found to depend on the interplay between ion energy and etch rate, with faster etch rates reducing the depth of the remaining damaged region. The maximum damage depth observed experimentally from capacitance-voltage profiling on Schottky rectifiers was ~110 nm, well beyond the range of the ions in the Inductively Coupled Plasmas and emphasizing that rapid diffusion of point defects occurs into the sample during the etch step. On-state resistance was more affected than parameters like ideality factor or breakdown voltage, with a factor of 5 increase for high ion energy exposures. Reverse current density shoed the presence of trap-assisted space-charge-limited conduction. The reverse recovery time of the rectifiers, 22 ns, was unaffected by the dry etch damage, with a constant value of reverse recovery current of 3 mA.

Introduction

As with any emerging semiconductor technology, control of defects and doping are key to Ga_2O_3 maturing into a commercial success [1,2]. For example, the lack of native p-type doping capability has led to use of p-type oxides to form heterojunctions with n-type Ga_2O_3 [3-10]. Another key processing step is etching. Patterning of Ga_2O_3 is predominantly carried out by dry etching, given the general lack of a wet etching capability at room temperature [11-27] While the plasma etch rates are relatively low, they are sufficient for the mesa or trench depths needed in most current devices, principally UV photodetectors, lateral transistors for switching applications and various types of vertical rectifiers for power management systems. There has been little investigation to understand the depth to which ion-induced damage occurs under practical etching conditions. It is generally observed in other semiconductors that changes in electrical properties of the etched surface may extend much deeper than the range of the ions incident on that surface [28-30]. This is often ascribed to rapid diffusion of primary defects such as vacancies or interstitials [29].

Ga vacancies have been identified as the most important defect in most situations in n-type β-Ga_2O_3 [1, 31-40] Due to the monoclinic lattice, there are the vacancies associated with two different Ga sites, V_{Ga1} and V_{Ga2}, but also three other energetically favorable split vacancy configurations in which the V_{Ga} is shared between two Ga sites with a Ga_i between them [37]. In n-type material, V_{Ga} is a deep triple acceptor [1]. The formation energies of Ga interstitials, a deep triple donor, are not favorable in n-type Ga_2O_3. Oxygen atoms have three different sites in the monoclinic lattice, that can correspondingly produce deficient V_O with energy levels of 1.6 - 2.0 eV below the conduction band [31,32]. Since these donors are very deep, they cannot contribute to the n-type conductivity. oxygen interstitials (Oi) are generally neglected for their effects on the material properties [31-35]. While the calculated threshold energies for displacement are 28 eV for Ga and 14 eV for O [41], the recombination rate of the latter are much higher, leaving Ga defects as the main influence on the electrical properties of the β-Ga_2O_3.

In this paper we report the depths to which the electrical properties of the near-surface region of β-Ga_2O_3 are altered after plasma exposure. The maximum depth over which the carrier concentration is reduced is 110 nm and this depends on the trade-off between ion energy and etch rate. The damage is well beyond the range of the highest energy Ar ions that strike the surface during etching. Schottky rectifiers on which the rectifying contacts were deposited on the etched surface were employed as the device platform to probe the damage effects. The on-state resistance of these devices was the most-affected parameter as a result of accumulated etch damage.

Experimental

The β-Ga_2O_3 samples for etch rate measurements were (100) bulk, Sn-doped substrates, grown by the Edge-Fed Defined Growth method and purchased from Novel Crystal Technology (Saitama, Japan). The etch rates were measured on samples patterned with PR1045 photoresist and etched in a PlasmaTherm 790 Inductively Coupled Plasma reactor. Discharges with 15 sccm of BCl_3 and 5 sccm of Argon at a fixed pressure of 5mTorr were used to etch the Ga_2O_3. The ICP source power and rf chuck power were varied to change plasma density and ion energy, respectively and thus alter the etch rates. Etch rates were obtained by measuring the etch depth with a Tencor profilometer after the removal of the photoresist.

Rectifier structures consisted of vertical rectifiers consisting of a thick (10 μm), lightly doped (~10^{16} cm^{-3}) epitaxial layer on a conducting (001) surface orientation Sn-doped β-Ga_2O_3 single crystal substrate (Novel Crystal Technology, Japan). A full area Ti/Au backside Ohmic contact was formed by e-beam evaporation and was annealed at 550̊C for 1minute under N_2 ambient. After exposure of the front surface to BCl_3/Ar discharges, the Ni/Au Schottky contact metal (100 μm diameter) was deposited through lithography using S1808 photoresist and LOR 3B. The current-voltage (I-V) and capacitance-voltage (C-V) characteristics were recorded with a Tektronix 370-A curve tracer, 371-B curve tracer and an Agilent 4156C. The reverse recovery was measured on a pulse generator at a bias of 10V,

Results and Discussion

Figure 1 shows the etch rates of Ga_2O_3 in the BCl_3/Ar ICP discharges as a function of dc self-bias, which was varied by altering the ICP source power and rf chuck power. The former controls the ion density in the plasma while the latter controls the energies of the positive ions incident on the powered electrode. The predominant ions present are Ar^+, with a smaller fraction of BCl_3 fragments, as determined from separate mass spectrometry measurements on this tool. The resultant average ion energy is the sum of the dc self-bias and the plasma sheath potential [29]. The latter is ~23V under the conditions used in the experiments. Therefore, the ion energies range from ~150-425 eV over the range of conditions we examined.

Figure 2 (top) shows the current density-voltage characteristics from the rectifiers etched under different dc self-bias conditions, corresponding to different etch rates The etch rates and source and chuck powers for these conditions are listed in Table I, which also shows the ideality factors and on-state resistances of the rectifiers extracted from the forward I-V characteristics assuming thermionic emission as the predominant conduction mechanism in that regime. The forward current shows a decrease under most conditions due to an increase in barrier height. The most affected parameter is the on-state resistance, which increases about a factor of 5, as shown in Figure 2. This is a major problem for power devices, since a widely used figure of merit is the breakdown volage squared, divided by the on-resistance. The specific on-resistance $R_{on,sp}$, is given by

$$R_{on,sp} = (W_D)/e\mu_n N_D$$

where W_D is the depletion depth in the drift region of the rectifier, e is the electronic charge, μ_n is the electron mobility and N_D is the carrier density. Since the depletion depth increases due to a decrease in carrier density and mobility, the on-state resistance is degraded. The bottom of Figure 2 (bottom) shows the J-V data in linear form, which clearly shows the increase in on-resistance extracted from the slope of the plots.

Figure 3 shows the variation of ideality factor and on-resistance as a function of dc self-bias. The lines are shown to guide the eye and do not represent a functional dependence. While the ideality factor, a commonly used indicator of changes in near-surface properties in etch damage experiments show only a relatively minor change, the on-resistance changes are more significant.

Figure 4 (top) shows the reverse J-V characteristics as a function of the different dc self-biases employed. Note that the reverse current is deceased after etching due to the reduction of carrier concentration. Over a moderate range of reverse biases, the characteristics could be fit to space charge-limited current (SCLC) conduction in the presence of deep-level states, characterized by plateaus in the semi-logarithmic plots and a functional dependence of J α V^n.

These arise from space charge-limited current conduction in a near-insulator with trapping centers and thermally generated carriers [42,43]. The values of n> 4 at higher reverse biases indicate trap charge-limited SCLC with an exponential distribution of traps was dominant under those conditions [42].

. Figure 5 shows the dependence on dc self-bias during etching of reverse leakage current measured at -100V and the breakdown voltage, defined as the bias at which the current density was 1A. cm^{-2}. The reverse leakage current shows a major increase at 400V self-bias.

To establish the depth profile of carrier concentration in the depletion region of the rectifiers, the carrier profile was extracted from the slope of the capacitance -voltage characteristics. Figure 6 (top) shows the change in slope at low biases of the C^{-2}-V plots, indicating the carrier density changes with depth. The net free carrier profile n(x) was obtained from the relation [43]

$$n(x) = -(C^3)/e\varepsilon A^2)\ (\frac{dC}{dV})^{-1}$$

where C is the capacitance, e the electronic charge, ε the dielectric constant of Ga_2O_3, and A the contact area. Figure 6 (bottom) shows the carrier profiles for different self-biases during etching. The carrier concentration is reduced due to the introduction of deep acceptors that trap electrons from the conduction band. As indicated earlier, these are likely the Ga vacancies prevalent in ion damaged Ga_2O_3.

The maximum depth to which the carrier density is reduced is ~110nm.This is well beyond the projected range of Ar^+ ions present in the plasmas. Figure 7 shows a Stopping and Range of Ions in Matter (SRIM) Monte Carlo simulation of the implanted ion depth and damage profile [44]. We have assumed an approximate dose of 10^{15} cm^{-2}, based on the ion flux to the electrode and the etch time. Note that the maximum direct incorporation depth is < 5nm, much less than the distance over which changes to the carrier profile are observed. This indicated rapid diffusion of the point defects created at the etched surface during plasma exposure. The V_{Ga} species are known to diffuse rapidly in Ga_2O_3 and this may be enhanced in the presence of the high level of electronic excitation during the plasma exposure [31]. Notice that the damage depth depends not only on the dc self-bias but also on the etch rate, with faster etch rates leading to lower damage depths.

As shown in Figure 8, the reverse recovery time of ~22 ns was independent of the self-bias used during etching, with the reverse recovery current, Irr, also constant at -3 mA. Thus, the presence of plasma damage does not affect the switching characteristics of the rectifiers, only the figure-of-merit related to the increase in on-resistance.

Summary and Conclusions

The damage depth in Ga_2O_3 as a result of high ion density ICP etching has been established. The carrier concentration can be reduced to depths of 110 nm, more than two orders of magnitude larger than the range of directly implanted positive ions in the discharge. This is an indicator of rapid diffusion of point defects created at the etching surface by positive ion bombardment. The damage depth is a trade-off between ion energy and etch rate since the damaged region is more rapidly removed at higher etch rates. It should also be possible to remove the surface damage region by a wet etch clean-up after plasma etching, since wet etching is enhanced in damaged crystalline material.

Acknowledgments

The work at UF was performed as part of Interaction of Ionizing Radiation with Matter University Research Alliance (IIRM-URA*)*, sponsored by the Department of the Defense,

Defense Threat Reduction Agency under award HDTRA1-20-2-0002. The content of the information does not necessarily reflect the position or the policy of the federal government, and no official endorsement should be inferred. The work at UF was also supported by NSF DMR 1856662.

Data Availability

The data that supports the findings of this study are available within the article and its supplementary material.

Declarations

The authors have no conflicts to disclose.

References

1. J. B. Varley, A. Janotti, C. Franchini, and C.G. Van de Walle, Role of self-trapping in luminescence and p-type conductivity of wide-band-gap oxides, Physical Review B 85 (2012) 081109.
2. A. Goyal, A. Zakutayev, V. Stevanović, and S. Lany, Computational Fermi level engineering and doping-type conversion of Mg:Ga_2O_3 via three-step synthesis process, J. Appl. Phys. 129 (2021) 245704.
3. Tatsuro Watahiki, Yohei Yuda, Akihiko Furukawa, Mikio Yamamuka, Yuki Takiguchi, and Shinsuke Miyajima, Heterojunction p-Cu_2O/n-Ga_2O_3 diode with high breakdown voltage, Appl. Phys. Lett. 111 (2017) 222104.
4. J. Zhang, S. Han, M. Cui, X. Xu, W. Li, H. Xu, C. Jin, M. Gu, L. Chen and K.H. L. Zhang, Fabrication and Interfacial Electronic Structure of Wide Bandgap NiO and Ga_2O_3 p–n Heterojunction, ACS Appl. Electron. Mater. 2 (2020) 456-462.
5. Y. Lv, Y. Wang, X. Fu, Shaobo Dun, Z. Sun, Hongyu Liu, X. Zhou, X. Song, K. Dang, S. Liang, J. Zhang, H. Zhou, Z. Feng, S. Cai and Yue Hao, "Demonstration of β-Ga_2O_3 Junction barrier Schottky diodes with a Baliga's figure of merit of 0.85 GW/cm^2 or a 5A/700 V handling capabilities, IEEE Trans Power Electron. 36 (2021) 6179-6184.
6. H. H. Gong, X. H. Chen, Y. Xu, F.-F. Ren, S. L. Gu and J. D. Ye, A 1.86-kV double layered NiO/β-Ga_2O_3 vertical p–n heterojunction diode, Appl. Phys. Lett., 117 (2020) 022104.
7. X. Lu, Xianda Zhou, Huaxing Jiang, Kar Wei Ng, Zimin Chen, Yanli Pei, Kei May Lau and Gang Wang, 1-kV sputtered p-NiO/n-Ga_2O_3 heterojunction diodes with an ultra-low leakage current below1μA/cm^2, IEEE Electron Dev. Lett .41 (2020) 449-453.

8. Chinju Wang, Hehe Gong, Weina Lei, Y. Cai, Z. Hu, Shengrui Xu, Zhihong Liu, Qian Feng, Hong Zhou, Jiandong Ye, Jincheng Zhang, Rong Zhang, and Yue Hao, Demonstration of the p-NiOx/n-Ga_2O_3 Heterojunction Gate FETs and Diodes With BV^2/Ron,sp Figures of Merit of 0.39 GW/cm^2 and 1.38 GW/cm^2, IEEE Electron Dev. Lett, 42 (2021) 485-489.

9. Yuangang Wang, Hehe Gong, Yuanjie Lv, Xingchang Fu, Shaobo Dun, Tingting Han, Hongyu Liu, Xingye Zhou, Shixiong Liang, Jiandong Ye, Rong Zhang, Aimin Bu, Shujun Cai and Zhihong Feng, 2.41 kV Vertical P-Nio/n-Ga2O3 Heterojunction Diodes With a Record Baliga's Figure-of-Merit of 5.18 GW/cm^2, IEEE Trans. Power Electron. 37(2022) 3743-3748.

10. Jian-Sian Li, Chao-Ching Chiang, Xinyi Xia, Fan Ren, Honggyu Kim and S.J. Pearton, Demonstration of 4.7 kV breakdown voltage in NiO/$\boldsymbol{\beta}$-Ga_2O_3 vertical rectifiers, Appl. Phys. Lett. 121 (2022) 042105.

11. A.Y. Polyakov, I.H. Lee, N.B. Smirnov, E.B. Yakimov, I.V.Shchemerov, A.V. Chernykh, A.I. Kochkova, A.A. Vasilev, P.H. Carey, F. Ren, D.J. Smith, S.J. Pearton, Defects at the surface of β-Ga_2O_3 produced by Ar plasma exposure, APL Materials 7 (2019) 061102.

12. J. Yang, Z. Sparks, F. Ren, S. J. Pearton, and M. Tadjer, Effect of surface treatments on electrical properties of β-Ga_2O_3, J. Vac. Sci. Technol. B 36 (2018) 061201.

13. J. Yang, S. Ahn, F. Ren, R. Khanna, K. Bevlin, D. Geerpuram, S. J. Pearton and A. Kuramata, Inductively Coupled Plasma Etch Damage in (201) Ga_2O_3 Schottky Diodes, Appl. Phys. Lett.110 (2017) 142101.

14. B. Alhalaili, R. Vidu, H. Mao, O. Kamoun, M. Saif Islam, Photoelectrochemical (PEC) etching of Ga_2O_3, Ceram. Int. 47 (2021) 479–486.

15. S.L. Ou, D.S. Wuu, Y.C. Fu, S.P. Liu, R.H. Horng, L. Liu, Z.C. Feng, Growth and etching characteristics of gallium oxide thin films by pulsed laser deposition. Mater. Chem. Phys. 133 (2012) 700–705.

16. Y.H. Choi, K.H. Baik, S. Kim, J. Kim, Photoelectrochemical etching of ultra-wide bandgap β-Ga2O3 semiconductor in phosphoric acid and its optoelectronic device application. Appl. Surf. Sci. 539 (2021) 148130.

17. J. Yang, S. Ahn, F. Ren, S. Pearton, R. Khanna, K. Bevlin, D. Geerpuram, A. Kuramata, Inductively coupled plasma etching of bulk, single-crystal Ga_2O_3, J. Vac. Sci. Technol. B 35 (2017) 031205.

18. L. Zhang, A. Verma, H.G. Xing, D. Jena, Inductively-coupled plasma reactive ion etching of single-crystal β-Ga_2O_3. Jpn. J.Appl. Phys. 56 (2017) 030304.

19. Y. Kwon, G. Lee, S. Oh, J. Kim, S. J. Pearton and Fan Ren, Tuning the thickness of exfoliated quasi two dimensional β Ga_2O_3 flakes by plasma etching, Appl. Phys. Lett. 110 (2017) 131901.

20. J. E. Hogan, S. W. Kaun, E. Ahmadi, Y. Oshima, and J. S. Speck, Chlorine-based dry etching of β-Ga_2O_3, Semicond. Sci. Technol. 31 (2016) 065006.

21. Y. Zhang, A. Mauze, J. Speck, Anisotropic etching of β-Ga_2O_3 using hot phosphoric acid. Appl. Phys. Lett. 115 (2019) 013501.

22. Yuewei Zhang, Akhil Mauze, and James S. Speck, Anisotropic etching of β-Ga_2O_3 using hot phosphoric acid, Appl. Phys. Lett. 115 (2019) 013501.

23. Han Na Cho, Su Ryun Min, Hyung Jin Bae, Jung Hyun Lee, and Chee Won Chung, Etch Characteristics of Nickel Oxide Thin Films Using Inductively Coupled Plasma Reactive Ion Etching, Electrochem. Solid-State Lett., 11 (2008) D23.

24. A.P. Shah and A. Bhattacharya, Inductively coupled plasma reactive-ion etching of β-Ga_2O_3, J. Vac. Sci. Technol. 35 (2017) 041301.

25. S. Jang, S. Jung, K. Beers, J. Yang, F. Ren, A. Kuramata, S.J. Pearton and K.H. Baik, A comparative study of wet etching and contacts on (201) and (010) oriented β Ga_2O_3, J. Alloys Comp. 731 (2018)118-126.

26. Hironori Okumura and Taketoshi Tanaka, Dry and wet etching for β-Ga_2O_3, Schottky barrier diodes with mesa termination, Jpn. J. Appl. Phys. 58 (2019) 120902.

27. Hsien-Chih Huang, Zhongjie Ren, Clarence Chan, Xiuling Li, Wet etch, dry etch, and MacEtch of β-Ga_2O_3: A review of characteristics and mechanism, J. Mater. Res. 36 (2021) 4756.

28. C. Steinbruchel, Universal energy dependence of physical and ion-enhanced chemical etch yields at low ion energy, Appl. Phys. Lett. 55 (1989) 1960-1962.

29. S.J. Pearton, Erica A. Douglas, Randy J. Shul and F. Ren, Plasma etching of wide bandgap and ultrawide bandgap semiconductors, J. Vac. Sci. Technol. A 38 (2020) 020802 .

30. Xinyi Xia, Nahid Sultan Al Mamun, Maxwell Wetherington, Fan Ren, Aman Haque and S.J. Pearton, Ga^+ Focused Ion Beam Damage in n type Ga_2O_3,J. Vac. Sci. Technol. A 40 (2022) 053403.

31. Y.K. Frodason, J.B. Varley, K.M. Johansen, Lasse Vines and C.G.Van de Walle, Migration of Ga vacancies and interstitials in Ga_2O_3, Phys. Rev. B, 107 (2023) 024109.

32. M. E. Ingebrigtsen, J. B. Varley, A. Y. Kuznetsov, B. G. Svensson, G. Alfieri, A. Mihaila, U. Badstöbner, and L. Vines, Iron and intrinsic deep level states in Ga_2O_3, Appl. Phys. Lett. 112 (2018) 042104.

33. P. Weiser, M. Stavola, W. B. Fowler, Y. Qin, and S. Pearton, Structure and vibrational properties of the dominant O-H center in β-Ga_2O_3", Appl. Phys. Lett. 112 (2018) 232104.

34. Y. Qin, M. Stavola, W. B. Fowler, P. Weiser, and S. J. Pearton, Hydrogen Centers in β-Ga_2O_3: Infrared Spectroscopy and Density Functional Theory, ECS J. Solid State Sci. Technol. 8 (2019) Q3103-3108.

35. H. J. von Bardeleben, S. Zhou, U. Gerstmann, D. Skachkov, W. R. L. Lambrecht, Q. D. Ho, and P. Deák, Proton irradiation induced defects in β-Ga_2O_3: A combined EPR and theory study, APL Mater. 7 (2019) 022521.

36. Dmitry Skachkov, Walter R. L. Lambrecht, Hans Jürgen von Bardeleben, Uwe Gerstmann, Quoc Duy Ho, and Peter Deák, Computational identification of Ga-vacancy related electron paramagnetic resonance centers in β-Ga_2O_3, J. Appl. Phys. 125 (2019) 185701.

37. W. Beall Fowler, Michael Stavola, Ying Qin, and Philip Weiser, Trapping of multiple H atoms at the Ga(1) vacancy in β-Ga_2O_3, Appl. Phys. Lett. 117 (2020) 142101.

38. P. Deák, Q. Duy Ho, F. Seemann, B. Aradi, M. Lorke, and T. Frauenheim, Choosing the correct hybrid for defect calculations: A case study on intrinsic carrier trapping in β−Ga_2O_3, Phys. Rev. B 95(2017) 075208 .

39. B. E. Kananen, L. E. Halliburton, K. T. Stevens, G. K. Foundos and N. C. Giles, Gallium vacancies in β-Ga_2O_3 crystals, Appl. Phys. Lett. 110 (2017) 202104.

40. A. Karjalainen, V. Prozheeva, K. Simula, I. Makkonen, V. Callewaert, J. B. Varley, and F. Tuomisto, Split Ga vacancies and the unusually strong anisotropy of positron annihilation spectra in β-Ga_2O_3, Phys. Rev. B 102 (2020) 195207.

41. Blair R. Tuttle, Nathaniel J. Karom, Andrew O'Hara, Ronald D. Schrimpf, and Sokrates T. Pantelides, Atomic-displacement threshold energies and defect generation in irradiated β-Ga_2O_3: A first-principles investigation, J. Appl. Phys. 133 (2023) 015703.

42. F. Mott and R. W. Gurney, Electronic Processes in Ionic Crystals (Clarendon Press, 1948).

43. S. M. Sze, L. Yiming, and K. K. Ng, Physics of Semiconductor Devices, 3rd ed.(John Wiley & Sons, 2021).

44. http://www.srim.org/index.htm

Table 1. Electrical parameters of Ga_2O_3 rectifiers etched by BCl_3/Ar plasmas prior to Schottky contact deposition.

ICP (W)	**RF (W)**	**DC bias (V)**	**Etch rate (Å/min)**	**V_{on} (V)**	**R_{on} (mΩ/cm^2)**	**SBH (V)**	**Ideality factor**	**Leakage current at -100V (µA/cm^2)**	**Breakdown voltage (V)**
0	0	0	0	0.82	1.41	0.68	1.14	9.7	-597
400	50	130	410	0.82	1.96	0.75	1.05	6.7	-608
400	150	300	500	0.71	5.86	0.74	1.08	50.1	-627
400	200	400	510	0.75	7.59	0.71	1.10	236.2	-677
600	200	300	810	0.74	7.35	0.67	1.12	4.8	-678

Figure Captions

Figure 1. Correlation between the DC self-bias voltage during ICP etching and the etch rate of Ga_2O_3.

Figure 2. (top) Forward characteristics of rectifiers with different etching damage including log forward current density, turn-on voltage and on-state resistance (bottom) forward current density in linear plot.

Figure 3. Ideality factor and on-state resistance as a function of dc self-bias during etching.

Figure 4. Reverse characteristics of rectifiers with different etching damage including (top) reverse current density with polynomial fitting to $I \propto V^n$ and (bottom) breakdown voltage,

Figure 5. Leakage current at -100 V reverse bias and breakdown voltage under different etch bias conditions.

Figure 6. (top) Capacitance-voltage characteristics as a function of self-bias during etching (bottom) corresponding carrier depth profiles.

Figure 7. Calculated ion and damage profiles for 100 and 500 eV Ar^+ ions in Ga_2O_3.

Figure 8. Switching characteristics from a current of 100mA to OV bias with different amounts of damage in the devices.

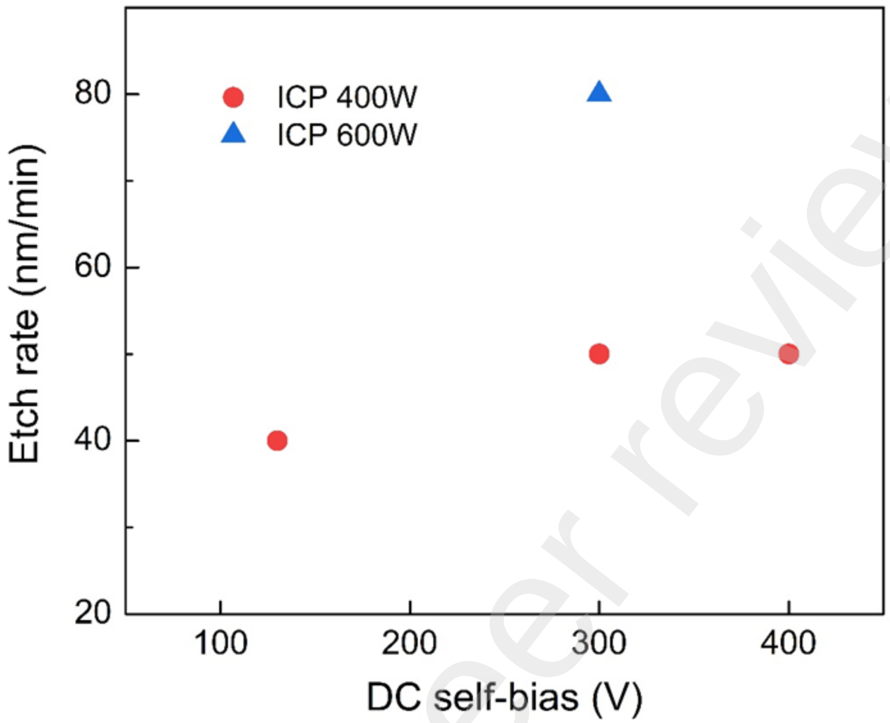

80
60
40
20
Etch rate (nm/min)
● ICP 400W
▲ ICP 600W
100
200
300
400
DC self-bias (V)

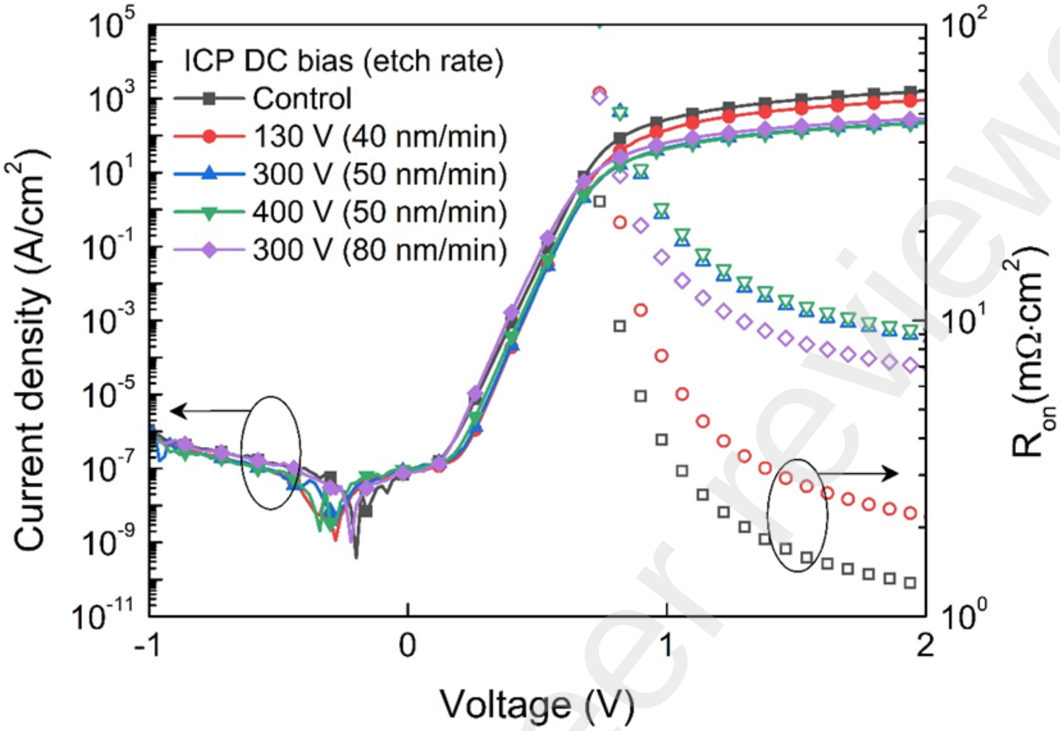
ICP DC bias (etch rate)
Control
130 V (40 nm/min)
300 V (50 nm/min)
400 V (50 nm/min)
300 V (80 nm/min)
Current density (A/cm^2)
R_{on} (mΩ·cm^2)
Voltage (V)
10^5
10^3
10^1
10^{-1}
10^{-3}
10^{-5}
10^{-7}
10^{-9}
10^{-11}
10^2
10^1
10^0
-1
0
1
2

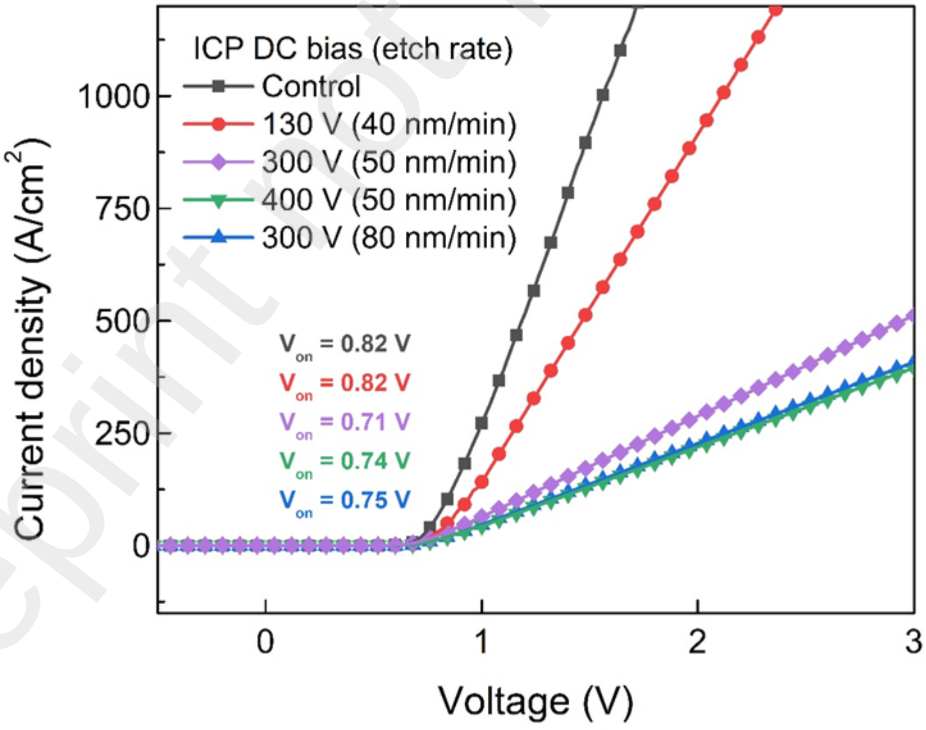
ICP DC bias (etch rate)
Control
130 V (40 nm/min)
300 V (50 nm/min)
400 V (50 nm/min)
300 V (80 nm/min)
V_{on} = 0.82 V
V_{on} = 0.82 V
V_{on} = 0.71 V
V_{on} = 0.74 V
V_{on} = 0.75 V
Current density (A/cm^2)
Voltage (V)
1000
750
500
250
0
0
1
2
3

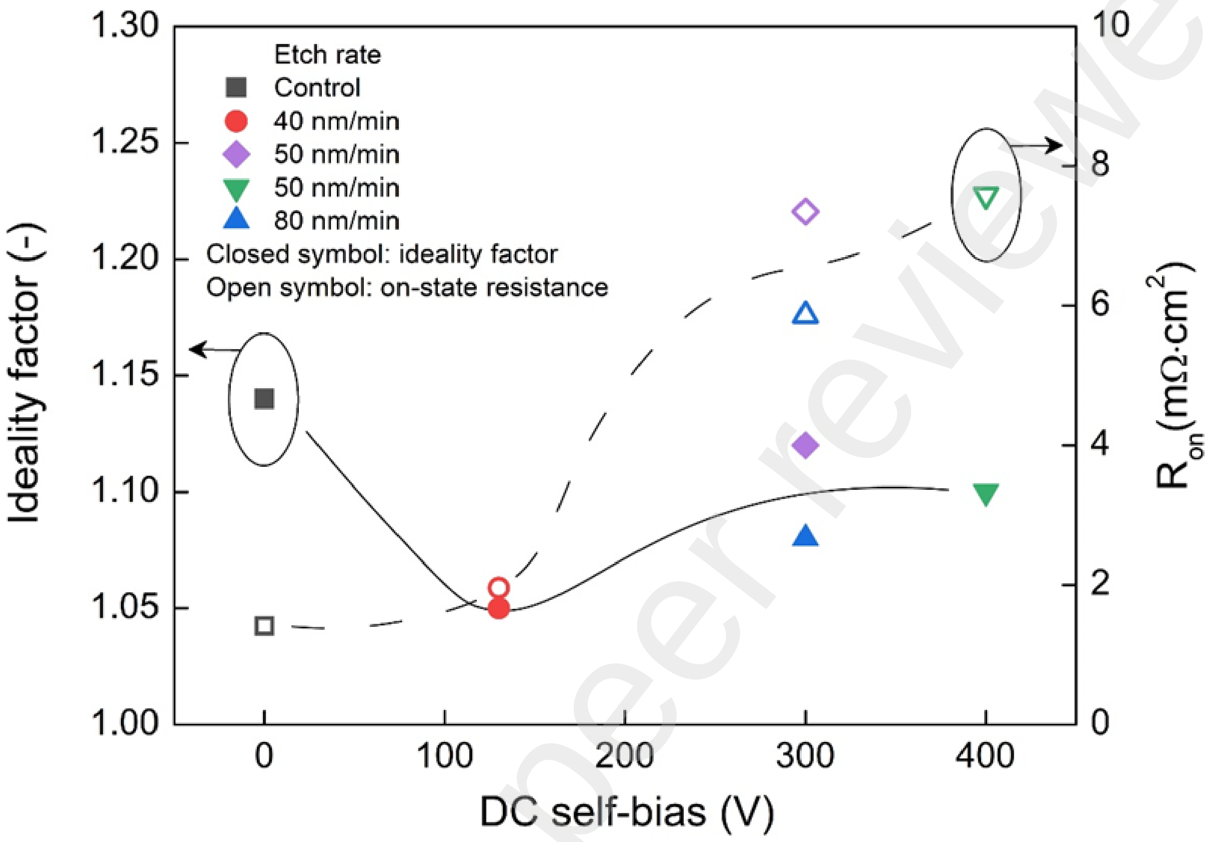

1.30
1.25
1.20
1.15
1.10
1.05
1.00
Ideality factor (-)
10
8
6
4
2
0
R_{on} (mΩ·cm^2)
0
100
200
300
400
DC self-bias (V)
Etch rate
■ Control
● 40 nm/min
◆ 50 nm/min
▼ 50 nm/min
▲ 80 nm/min
Closed symbol: ideality factor
Open symbol: on-state resistance

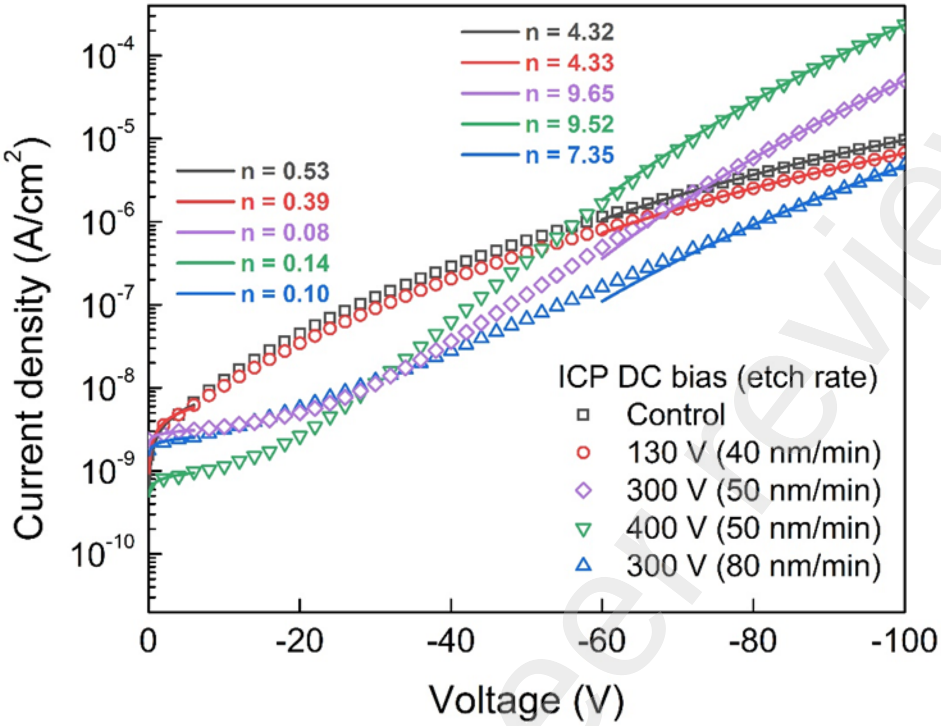
n = 4.32
n = 4.33
n = 9.65
n = 9.52
n = 7.35
n = 0.53
n = 0.39
n = 0.08
n = 0.14
n = 0.10
ICP DC bias (etch rate)
Control
130 V (40 nm/min)
300 V (50 nm/min)
400 V (50 nm/min)
300 V (80 nm/min)
Current density (A/cm^2)
10^{-4}
10^{-5}
10^{-6}
10^{-7}
10^{-8}
10^{-9}
10^{-10}
0
-20
-40
-60
-80
-100
Voltage (V)

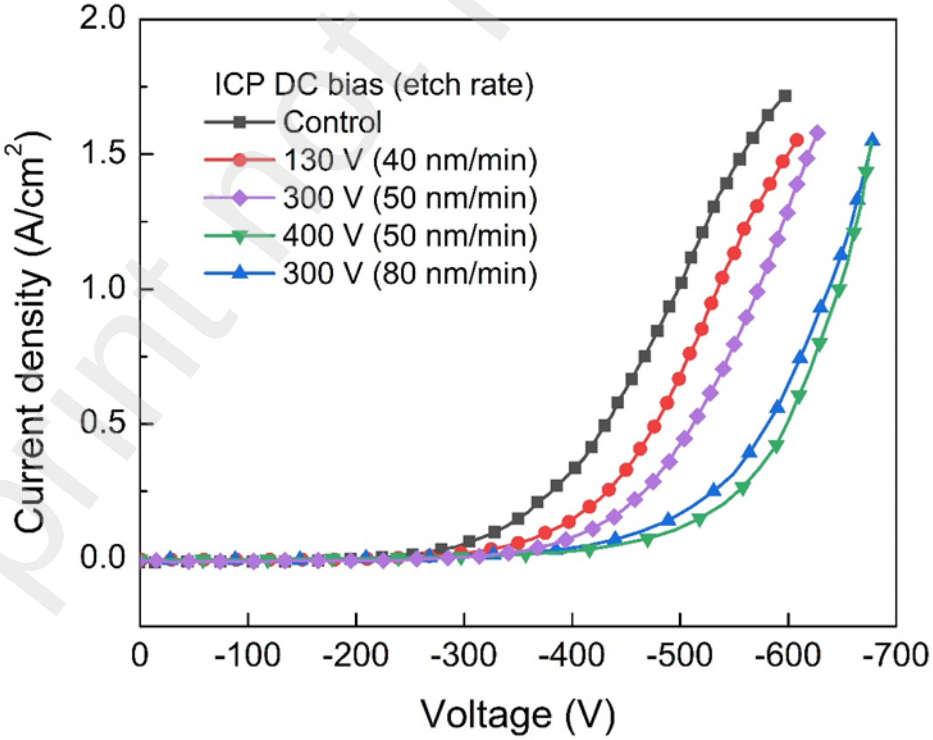
ICP DC bias (etch rate)
Control
130 V (40 nm/min)
300 V (50 nm/min)
400 V (50 nm/min)
300 V (80 nm/min)
Current density (A/cm^2)
2.0
1.5
1.0
0.5
0.0
0
-100
-200
-300
-400
-500
-600
-700
Voltage (V)

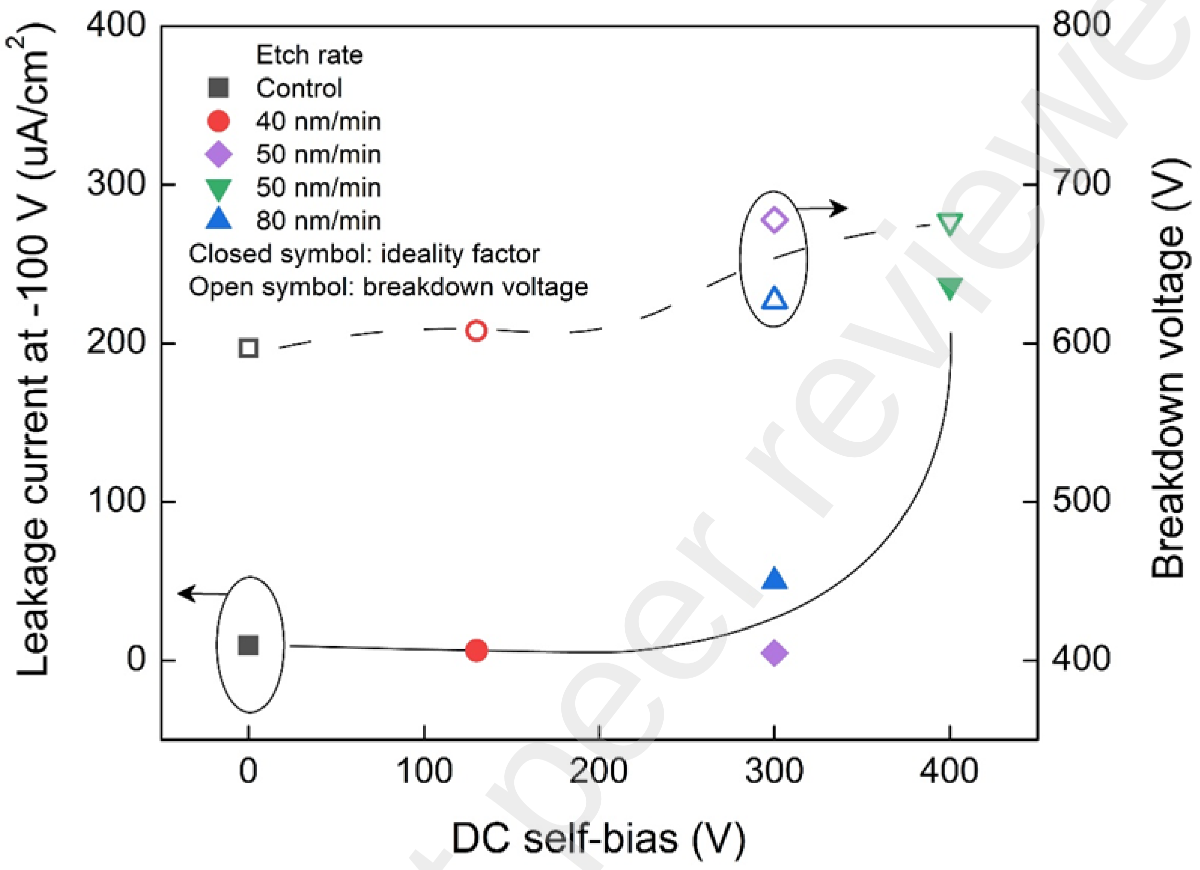

Etch rate
■ Control
● 40 nm/min
◆ 50 nm/min
▼ 50 nm/min
▲ 80 nm/min
Closed symbol: ideality factor
Open symbol: breakdown voltage
Leakage current at -100 V (uA/cm^2)
Breakdown voltage (V)
DC self-bias (V)
0
100
200
300
400
500
600
700
800

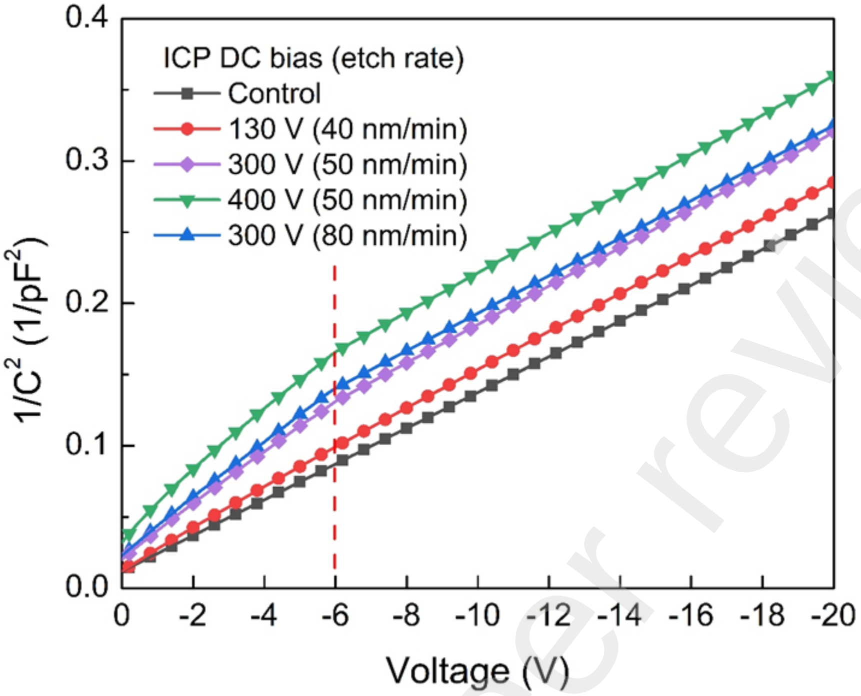
ICP DC bias (etch rate)
Control
130 V (40 nm/min)
300 V (50 nm/min)
400 V (50 nm/min)
300 V (80 nm/min)
$1/C^2$ (1/pF^2)
0.0
0.1
0.2
0.3
0.4
0
-2
-4
-6
-8
-10
-12
-14
-16
-18
-20
Voltage (V)

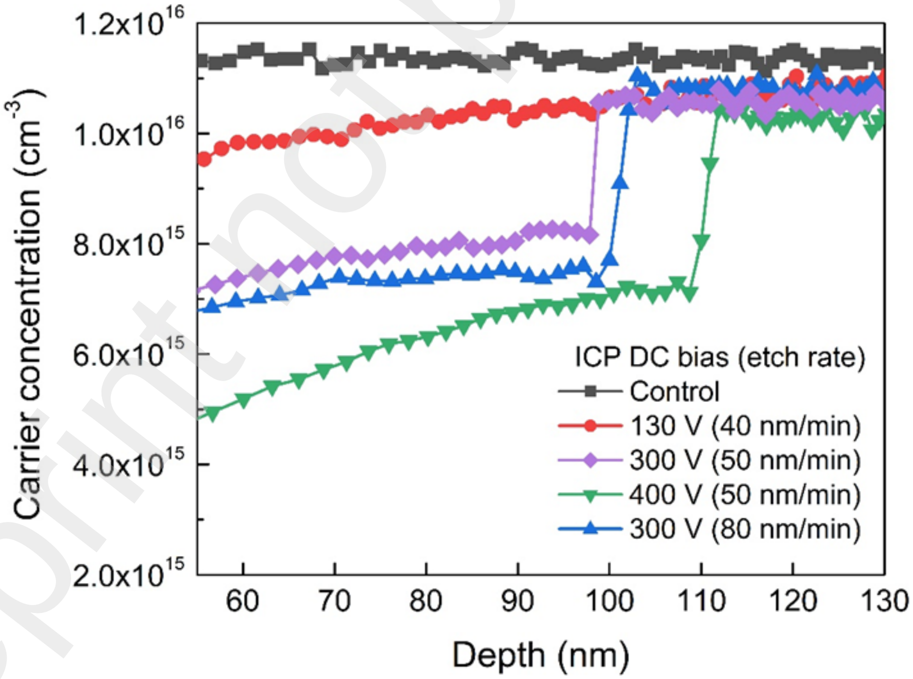
ICP DC bias (etch rate)
Control
130 V (40 nm/min)
300 V (50 nm/min)
400 V (50 nm/min)
300 V (80 nm/min)
Carrier concentration (cm^{-3})
$1.2x10^{16}$
$1.0x10^{16}$
$8.0x10^{15}$
$6.0x10^{15}$
$4.0x10^{15}$
$2.0x10^{15}$
60
70
80
90
100
110
120
130
Depth (nm)

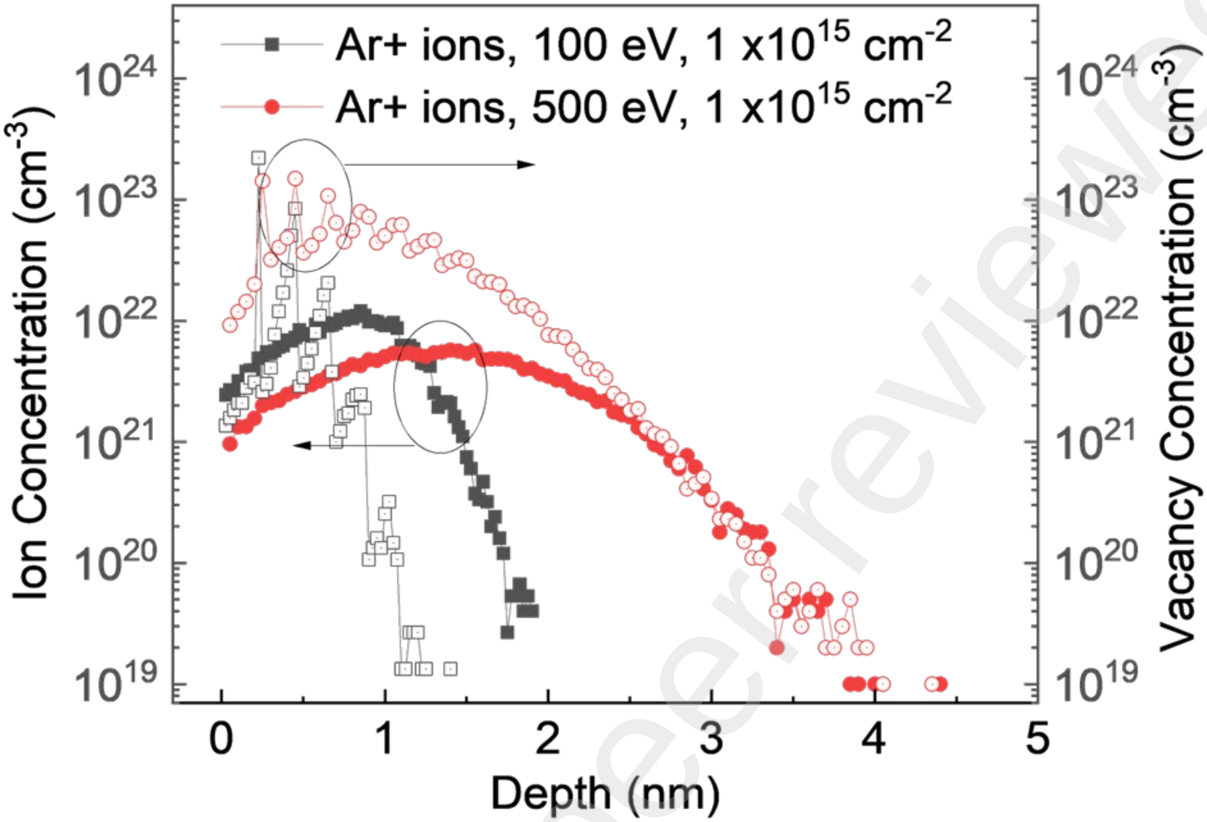
Ar+ ions, 100 eV, 1 x10^{15} cm^{-2}
Ar+ ions, 500 eV, 1 x10^{15} cm^{-2}
Ion Concentration (cm^{-3})
Vacancy Concentration (cm^{-3})
Depth (nm)
10^{24}
10^{23}
10^{22}
10^{21}
10^{20}
10^{19}
0
1
2
3
4
5

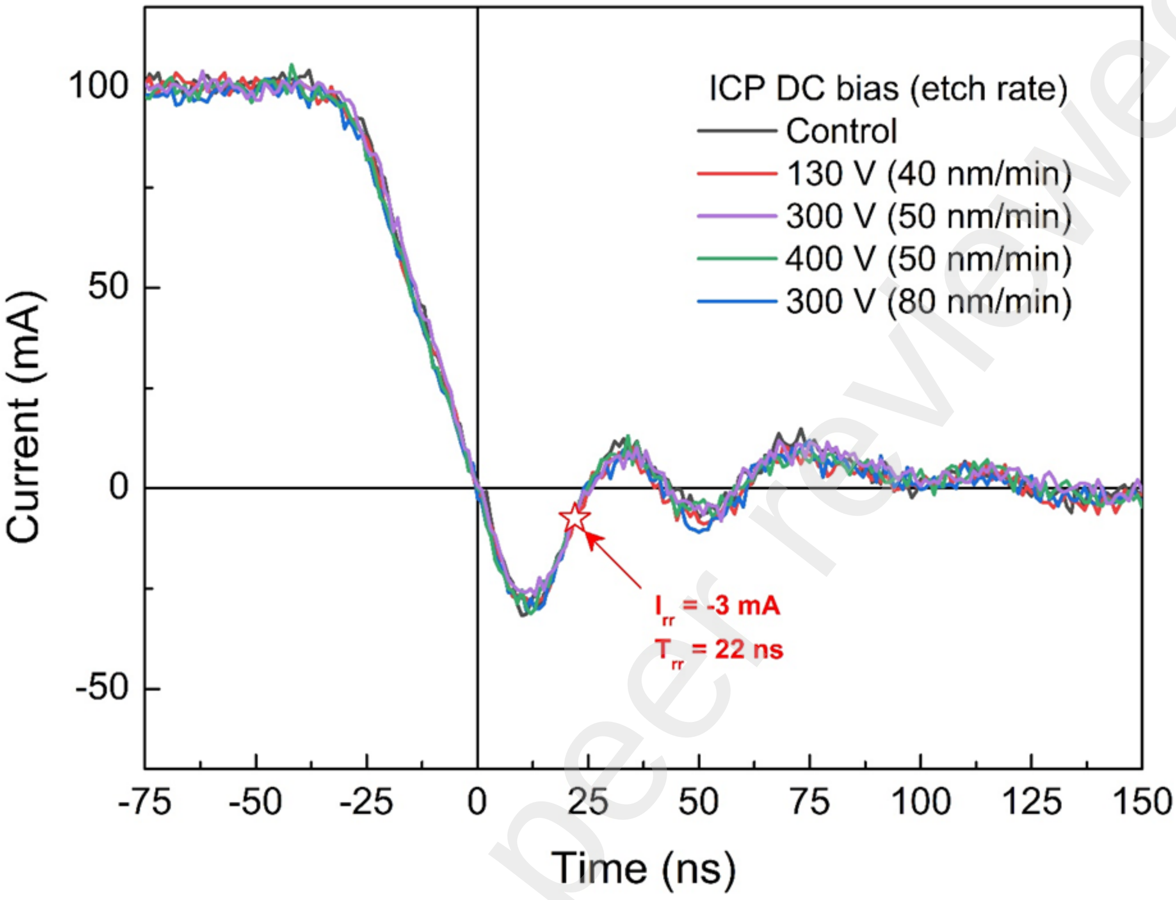
ICP DC bias (etch rate)
Control
130 V (40 nm/min)
300 V (50 nm/min)
400 V (50 nm/min)
300 V (80 nm/min)
I_{rr} = -3 mA
T_{rr} = 22 ns
Current (mA)
100
50
0
-50
-75
-50
-25
0
25
50
75
100
125
150
Time (ns)